Available online at www.sciencedirect.com
ScienceDirect
Journal of Sound and Vibration 307 (2007) 226–249
JOURNAL OF SOUND AND VIBRATION
www.elsevier.com/locate/jsvi

Structural damage identification in plates using spectral strain energy analysis

W.L. Bayissa*, N. Haritos

Department of Civil & Environmental Engineering, The University of Melbourne, Grattan Street, Parkville, Victoria 3010, Australia

Received 1 November 2006; received in revised form 19 June 2007; accepted 30 June 2007

Abstract

In this paper, a vibration response parameter known as spectral strain energy (SSE) is proposed for structural damage identification in plate-like structures in the context of a non-model-based damage identification approach. The SSE presented in this study is derived from moment–curvature response in which all the modal parameters (namely natural frequency, mode shapes and modal damping) are taken into account. First, displacement response power spectral density obtained from a plate element is used to determine moment power spectral density (MSD) and curvature power spectral density (CSD). A statistical parameter known as mean-square value (MSV) of the response spectral density is then obtained and used to derive SSE based on the assumption that the excitation force is a stationary, ergodic random noise. Consequently, various damage indices are computed and employed for damage detection and localization in simply supported plate and beam elements. The level of sensitivity to damage and performance of the SSE method is illustrated using extensive numerical simulation studies and by comparing the results with those obtained from the modal strain energy (MSE) method. Moreover, the performance and robustness of the SSE method is verified using the experimental modal data obtained from a full-scale bridge structure.

1. Introduction

In many areas of engineering applications such as aerospace, automotive, civil and mechanical engineering, plate elements are widely used as an important structural component. They are known for resisting lateral loads through flexural stiffness coupled with shear resistance. Analysis and design of plates subjected to lateral, in-plane, and combined lateral and in-plane loads are typically encountered in many engineering applications. Therefore, structural condition evaluation of plate-like elements that may be initiated due to stiffness degradation during in-service loading is an important aspect of global structural health assessment. In particular, structural condition monitoring becomes a critical issue after the occurrence of extreme events such as earthquakes and impact loads to avoid the possible loss of human lives due to undetected structural damage. In the last few decades, techniques based on vibration responses have been widely used for damage

*Corresponding author. Tel.: +61 3 8344 4709; fax: +61 3 8344 4616.
E-mail addresses: w.bayissa@civenv.unimelb.edu.au, wrtlem@yahoo.com (W.L. Bayissa), n.haritos@civenv.unimelb.edu.au (N. Haritos).

0022-460X/$ - see front matter © 2007 Elsevier Ltd. All rights reserved.
doi:10.1016/j.jsv.2007.06.062

identification and health monitoring. The premise for these techniques is that damage causes a change in structural physical properties, mainly in stiffness and damping at the damaged locations. These changes in structural properties in turn alter the dynamic response behaviour of the structure from its initial state. Therefore, monitoring of the changes in structural response parameters can be an important tool for the assessment of structural integrity by identifying damage at the earliest possible stage.

Based on the technique used to treat the measured responses for damage identification, the methodology used can be classified as either a "non-model-based" or "model-based" method. The model-based methods are capable of dealing with all damage levels such as localization and quantification of damage severity. However, these methods are computationally intensive, require updated numerical models and involve solution of inverse problems which are usually ill-conditioned. Therefore, the effectiveness of this approach is usually limited by insufficient measurement information and associated uncertainties (such as model error, measurement noise and low sensitivity of the response parameters to model parameter variations).

On the other hand, non-model-based methods are often used to identify and localize damage based on two sets of data—from the undamaged and the damaged states. Though limited levels of damage studies can be considered using this latter approach, there are nonetheless many advantages in using it. This approach is computationally simple and does not require an updated numerical model to implement. Extensive literature reviews on range of vibration-based damage identification techniques have previously been reported [1]. It is found that there are different response parameters implemented for non-model-based damage identification depending upon the approach adopted. These response parameters include natural frequency [2], mode shape curvatures [3], modal flexibility and its derivatives [4–6], modal stiffness [7], modal strain energy (MSE) [8], frequency response function (FRF) [9], FRF curvatures [10], pseudo-modal energy [11] and power spectral density (PSD) [12].

Even though numerous techniques and various response parameters have been used for damage identification studies, most of them are developed for one-dimensional structures, such as beams, frames and truss structures. Comparatively few studies are reported in the literature regarding damage identification on two-dimensional plate-like structures. Cawley and Adams [2] were probably the first who developed a damage detection algorithm for plate structures based on frequency shifts. Cornwell et al. [8] extended the modal energy method which was originally developed for damage detection in one-dimensional structures to plate structures. Chen and Bicanic [13] presented a damage identification algorithm for continuum structures by using natural frequencies and mode shapes in the context of an optimization technique. Lee and Shin [14] presented a methodology for damage identification in plates using measured modal data from the undamaged state and FRF from the damaged state of the structure investigated. Li et al. [15] presented a strain mode technique for damage identification in plate-like structures. Yam et al. [16] conducted a sensitivity analysis on static and dynamic response parameters used for damage identification in plate-like structures. Recently, Wu and Law [17] presented damage identification in plate structures based on changes in uniform load surface. Yoon et al. [18] extended the "gapped-smoothing" method originally developed for damage detection in one-dimensional structures to two-dimensional plate-like structures. Swamidas and Chen [19] presented a modal analysis technique using strain and acceleration measurements to detect crack growth in a cantilever plate.

In this paper, spectral strain energy (SSE) is proposed as a sensitive and effective damage indicator for damage identification in two-dimensional plate-like structures. SSE derived from two parameters known as moment response power spectral density (MSD) and curvature response power spectral density (CSD) is implemented in the context of a non-model-based approach where damage detection and localization is the main focus. The method can also be used to monitor both global and local changes in structures simultaneously by implementing the use of local sensors at critical locations and a grid of sensors at convenient locations to capture local and global structural responses during experimental modal testing. In the past, Cornwell et al. [8] presented a similar technique based on MSE which is derived from the mode shapes obtained from undamaged and damaged states to identify structural damage using a statistical hypothesis test. However, Cornwell et al. [8] have reported that the MSE method is not able to identify all multiple damage locations and in some cases false positive damages were identified. The drawback of MSE is that firstly mode shapes are not sufficient by themselves to identify damage since they are too sensitive to noise and contain only resonance frequency information. Secondly, other important resonance parameters such as natural frequencies and damping are not taken into account. Thirdly, this method always depends on experimental

modal analysis for its implementation. In contrast, the proposed method which is based on spectral analysis has many advantages: it takes into account all modal parameters; input–output and output-only damage identification investigations can be conducted with the only assumption that the excitation force is stationary, ergodic white noise; and this method is more flexible since it can also be implemented in the frequency domain as well as the modal domain. In this study, first the SSE is determined at each of the simulated measurement grid points for the damaged and undamaged states. Second, different damage indices that include relative changes in the mean-square value (MSV) of the response SSE, normalized damage index and relative root mean-square error (RRMSE) are computed and used to identify damage. Finally, a relative performance comparison is conducted between the proposed method and the MSE approach by applying structural damage identification on both plate and beam elements.

2. Strain energy analysis for plates

The general expression for the strain energy stored in a linear elastic system due to applied external forces can be found in most engineering textbooks, and is given by

$$U = \frac{1}{2}\int_V \{\sigma\}^{\mathrm{T}}\{\varepsilon\}\,\mathrm{d}V, \tag{1}$$

in which $\{\sigma\}^{\mathrm{T}} = \left\{\begin{array}{cccccc}\sigma_{xx} & \sigma_{yy} & \sigma_{zz} & \tau_{xy} & \tau_{xz} & \tau_{yz}\end{array}\right\}$; $\{\varepsilon\}^{\mathrm{T}} = \left\{\begin{array}{cccccc}\varepsilon_{xx} & \varepsilon_{yy} & \varepsilon_{zz} & \gamma_{xy} & \gamma_{xz} & \gamma_{yz}\end{array}\right\}$, where σ and ε are stress resultants and strains, respectively. U is the total potential or strain energy. Eq. (1) is based on linear elastic constitutive relations at the material level (stress–strain relations). However, in this paper the intention is to use an equation analogous to Eq. (1) but based on constitutive relations at the structural level, such as a curvature–moment relation and a shear stress–shear strain deformation relation. Therefore, the strain energy for an isotropic plate can be expressed in terms of stress resultants, curvatures and shear deformations using Reissner–Mindlin plate theory as follows [20]:

$$U = \frac{1}{2}\int_A (\mathbf{M}^{\mathrm{T}}\boldsymbol{\kappa} + \mathbf{Q}^{\mathrm{T}}\boldsymbol{\chi})\,\mathrm{d}A, \tag{2}$$

where $\mathbf{M}$ and $\boldsymbol{\kappa}$ are moment resultants and curvatures, respectively. $\mathbf{Q}$ and $\boldsymbol{\chi}$ are transverse shear stress resultants and shear deformations, respectively.

The constitutive relations relating stress resultants to the strains (curvatures) are given by

$$\mathbf{M} = \left\{\begin{array}{c}M_x\\M_y\\M_{xy}\end{array}\right\} = D\begin{bmatrix}1 & \upsilon & 0\\ \upsilon & 1 & 0\\ 0 & 0 & (1-\upsilon)/2\end{bmatrix}\left\{\begin{array}{c}\kappa_x\\\kappa_y\\\kappa_{xy}\end{array}\right\}, \quad \boldsymbol{\kappa} = \left\{\begin{array}{c}\kappa_x\\\kappa_y\\\kappa_{xy}\end{array}\right\} = \left\{\begin{array}{c}-\dfrac{\partial^2 w}{\partial x^2}\\ -\dfrac{\partial^2 w}{\partial y^2}\\ -\dfrac{2\partial^2 w}{\partial x \partial y}\end{array}\right\}, \tag{3}$$

$$\mathbf{Q} = \left\{\begin{array}{c}Q_x\\Q_y\end{array}\right\} = \frac{D}{h^2}\begin{bmatrix}6\alpha(1-\upsilon) & 0\\ 0 & 6\alpha(1-\upsilon)\end{bmatrix}\left\{\begin{array}{c}\chi_x\\\chi_y\end{array}\right\}, \tag{4}$$

where M_x and M_y are the flexural bending moments per unit width along the y- and x-axis, respectively, M_{xy} is the twisting moment, w the plate lateral deflection, α the shear correction factor and D the plate rigidity. For isotropic materials, $D = Eh^3/12(1-\upsilon^2)$, where E is the Young's modulus, υ the Poisson's ratio and h the plate thickness.

In this study, the amount of strain energy stored due to shear deformation will be neglected, only the strain energy corresponding to bending and twisting moments and the corresponding curvatures are taken into account.

2.1. SSE analysis for plate bending problems

In this paper, a response parameter known as SSE is implemented for structural damage identification. SSE is determined from bending MSD and CSD. The following assumptions are made to obtain MSDs and CSDs: (i) the structure is assumed to be lightly damped; (ii) modes are well-separated; (iii) sufficient number of significant modes are identified and used to generate respective response parameters; (iv) the unknown input PSD is assumed to be stationary ergodic random white noise, i.e., statistical properties of the input PSD remain constant for all damage conditions. Therefore, the SSE proposed in this paper is given by statistical properties of MSD and CSD, as follows:

$$U = \frac{1}{2}\int_A (\{\sigma_M^2\}^{\mathrm{T}}\{\sigma_\kappa^2\})\,\mathrm{d}A \tag{5}$$

where σ_M^2 and σ_κ^2 are MSVs of MSD and CSD, respectively.

The statistical properties σ_M^2 and σ_κ^2, known as zero-order spectral moment or mean power of MSD and CSD are computed using the formula widely used in random vibration theory for zero-mean Gaussian spectral density [21]:

$$\sigma_M^2 = \frac{1}{2\pi}\int_{-\infty}^{\infty} S_{MM}(\omega)\,\mathrm{d}\omega; \quad \sigma_\kappa^2 = \frac{1}{2\pi}\int_{-\infty}^{\infty} S_{\kappa\kappa}(\omega)\,\mathrm{d}\omega, \tag{6}$$

where $S_{MM}(\omega)$ and $S_{\kappa\kappa}(\omega)$ are response MSD and CSD, respectively. ω is the circular frequency.

2.3. Analysis of MSD and CSD for plate bending problem

For a linear system and a stationary random process, input–output relationships for MSD, CSD and MSV are obtained from the theory of random vibrations as [21]

$$S_{MM}(j,l,\omega) = |H_M(j,l,\omega)|^2 S_{ff}(l,\omega); \quad S_{\kappa\kappa}(j,l,\omega) = |H_\kappa(j,l,\omega)|^2 S_{ff}(l,\omega), \tag{7}$$

where $S_{ff}(l,\omega) = |F(l,\omega)|^2$; $F(l,\omega) = \int_{-\infty}^{\infty} f(x,y,t)\mathrm{e}^{-\mathrm{i}\omega t}\,\mathrm{d}t$; $S_{MM}(j,l,\omega)$ and $S_{\kappa\kappa}(j,l,\omega)$ are MSD and CSD at grid point j due to excitation at point l. $H_M(j,l,\omega)$ and $H_\kappa(j,l,\omega)$ are the FRFs for moment and curvature responses, respectively. $S_{\mathrm{ff}}(l,\omega)$ is the input PSD; $f(x,y,t)$ is the input excitation force; and $F(l,\omega)$ is the corresponding Fourier spectrum.

2.3.1. Determination of moment and curvature FRFs

The FRF is a measure of the steady-state response to harmonic excitation at a frequency ω. For the bending moment and curvature responses measured at a point, say $j(x, y)$ due to a harmonic excitation force applied at a point $l(x = r, y = s)$, the corresponding FRFs can be described by the following equation:

$$H_M(j,l,\omega) = \frac{\mathrm{FT}(M(j,t))}{\mathrm{FT}(f(l,t))}, \quad H_\kappa(j,l,\omega) = \frac{\mathrm{FT}(\kappa(j,t))}{\mathrm{FT}(f(l,t))}, \tag{8}$$

where $M(j,t)$ and $\kappa(j,t)$ are bending/twisting moment and curvature responses, respectively. $\mathrm{FT}(\cdot)$ represents the Fourier transformation of the respective response parameters. There are two possible approaches to obtain the bending moment FRF: (i) directly from experimental strain measurements and (ii) indirectly from displacement or acceleration responses from accelerometer measurements. In this paper, the latter option is adopted where the moment FRF can be obtained from superposition of normal modes or from fast Fourier transformation (FFT) analysis. The main advantage of this approach is that the method can be applied to experimental modal testing where a limited number of modes can be measured in practice and provides an option to include modes that most contribute to the overall response of the structure.

2.3.2. Determination of displacement response for plates

For an elastic, isotropic and thin rectangular plate subjected to uniform lateral excitation forcing, the dynamic equation of motion is given by [22]

$$D\left(\frac{\partial^4 w}{\partial x^4} + 2\frac{\partial^4 w}{\partial x^2 \partial y^2} + \frac{\partial^4 w}{\partial y^4}\right) + C\frac{\partial w}{\partial t} + \bar{m}\frac{\partial^2 w}{\partial t^2} = f(x,y,t), \tag{9}$$

where $w(x, y, t)$ is the lateral deflection at location (x, y) and time t. $f(x, y, t)$ is an arbitrary vertical excitation force. C and $\bar{m}$ are viscous damping coefficient and mass density per unit area, respectively. Assuming that a lateral excitation load is applied at a point $l(x = r, y = s)$ and is varying harmonically with time, the equivalent distributed load per unit area can be described by

$$f(x, y, t) = F_0(x, y)\mathrm{e}^{\mathrm{i}\omega t}\delta(x - r)\delta(y - s),$$

where F_0 is the amplitude of the harmonic point load; $\delta(\cdot)$ is the Dirac's delta function; and ω is the circular frequency of the forcing function. Similarly, the forced vibration response of an intact plate to steady-state oscillation can be assumed to be varying harmonically with time and can be obtained by superposition of its undamped natural modes multiplied by the natural coordinates, in the form

$$w(x, y, t) = \sum_{m=1}^{\infty}\sum_{n=1}^{\infty}\psi_{mn}(x, y)\theta_{mn}(t),$$

where ψ_{mn} and θ_{mn} are the natural modes and generalized coordinates, respectively. Consequently, the forced vibration response of the undamaged plate can be obtained using the normal mode analysis by substituting $f(x, y, t)$ and $w(x, y, t)$ into Eq. (9) and using the orthonormality conditions, as follows:

$$w(x, y, t) = \sum_{m=1}^{\infty}\sum_{n=1}^{\infty}\frac{\phi_{mn}(x, y)\phi_{mn}(r, s)}{\left(\omega_{mn}^2 + \beta_{mn}i\omega - \omega^2\right)}F_0(r, s)\mathrm{e}^{\mathrm{i}\omega t}, \tag{10}$$

where ϕ_{mn} are the mass-normalized mode shapes, $\phi_{mn} = \psi_{mn}/\sqrt{\bar{m}_{mn}}$ and $\phi_{mn}^{\mathrm{T}}\bar{m}\phi_{mn} = 1$. β_{mn} are the modal bandwidths, $\beta_{mn} = c_{mn}/\bar{m}_{mn} \approx 2\mathrm{i}\zeta_{mn}\omega_{mn}$; $\bar{m}_{mn}$ and c_{mn} are the modal masses and damping coefficients, respectively; ζ_{mn} are the modal damping ratios; and ω_{mn} are the natural circular frequencies. Therefore, by substituting Eq. (10) back into Eqs. (3) and (8) consecutively, the bending moment, twisting moment and curvature FRFs can be obtained. As a result, the bending/twisting MSDs and CSDs are obtained from Eq. (7), as follows:

(a) MSD functions:

$$S_{MMx}(j, l, \omega) = \left|H_{Mx}(j, l, \omega)\right|^2 S_{ff}(l, \omega) = D^2\sum_{m=1}^{\infty}\sum_{n=1}^{\infty}\frac{\left(\dfrac{\partial^2\phi_{mn}^j}{\partial x^2} + \upsilon\dfrac{\partial^2\phi_{mn}^j}{\partial y^2}\right)^2(\phi_{mn}^l)^2}{(\omega_{mn}^2 - \omega^2)^2 + (\beta_{mn}\omega)^2}S_{ff}(l, \omega), \tag{11}$$

$$S_{MMy}(j, l, \omega) = |H_{My}(j, l, \omega)|^2 S_{ff}(l, \omega) = D^2\sum_{m=1}^{\infty}\sum_{n=1}^{\infty}\frac{\left(\dfrac{\partial^2\phi_{mn}^j}{\partial y^2} + \upsilon\dfrac{\partial^2\phi_{mn}^j}{\partial x^2}\right)^2(\phi_{mn}^l)^2}{(\omega_{mn}^2 - \omega^2)^2 + (\beta_{mn}\omega)^2}S_{ff}(l, \omega), \tag{12}$$

$$S_{MMxy}(j, l, \omega) = |H_{Mxy}(j, l, \omega)|^2 S_{ff}(l, \omega) = \left(\frac{1 - \upsilon}{2}\right)^2 D^2\sum_{m=1}^{\infty}\sum_{n=1}^{\infty}\frac{\left(2\dfrac{\partial^2\phi_{mn}^j}{\partial x\partial y}\right)^2(\phi_{mn}^l)^2}{(\omega_{mn}^2 - \omega^2)^2 + (\beta_{mn}\omega)^2}S_{ff}(l, \omega). \tag{13}$$

(b) CSD functions:

$$S_{\kappa\kappa x}(j, l, \omega) = \left|H_{\kappa x}(j, l, \omega)\right|^2 S_{ff}(l, \omega) = \sum_{m=1}^{\infty}\sum_{n=1}^{\infty}\frac{\left(\dfrac{\partial^2\phi_{mn}^j}{\partial x^2}\right)^2(\phi_{mn}^l)^2}{(\omega_{mn}^2 - \omega^2)^2 + (\beta_{mn}\omega)^2}S_{ff}(l, \omega), \tag{14}$$

$$S_{\kappa\kappa y}(j,l,\omega) = \left|H_{\kappa y}(j,l,\omega)\right|^2 S_{ff}(l,\omega) = \sum_{m=1}^{\infty}\sum_{n=1}^{\infty} \frac{\left(\frac{\partial^2 \phi_{mn}^{j}}{\partial y^2}\right)^2 (\phi_{mn}^{l})^2}{(\omega_{mn}^2 - \omega^2)^2 + (\beta_{mn}\omega)^2} S_{ff}(l,\omega), \tag{15}$$

$$S_{\kappa\kappa xy}(j,l,\omega) = \left|H_{\kappa xy}(j,l,\omega)\right|^2 S_{ff}(l,\omega) = \sum_{m=1}^{\infty}\sum_{n=1}^{\infty} \frac{\left(2\frac{\partial^2 \phi_{mn}^{j}}{\partial x \partial y}\right)^2 (\phi_{mn}^{l})^2}{(\omega_{mn}^2 - \omega^2)^2 + (\beta_{mn}\omega)^2} S_{ff}(l,\omega), \tag{16}$$

where $H_{Mx}(j,l,\omega)$, $H_{My}(j,l,\omega)$ and $H_{Mxy}(j,l,\omega)$ are the moment FRFs along the x-axis, y-axis and x–y-axis, respectively. $H_{\kappa x}(j,l,\omega)$, $H_{\kappa y}(j,l,\omega)$ and $H_{\kappa xy}(j,l,\omega)$ are the curvature FRFs along the x-axis, y-axis and x–y-axis, respectively.

2.4. Determination of moment and curvature MSVs

The MSVs for MSDs and CSDs are determined by substituting Eqs. (11)–(16) into Eq. (6) as follows:

(a) MSV of MSD functions:

$$\sigma_{Mx}^2(j,l) = \left(\frac{D^2}{2\pi}\right) \times \int_{-\infty}^{\infty} \sum_{m=1}^{\infty}\sum_{n=1}^{\infty} \frac{\left(\frac{\partial^2 \phi_{mn}^{j}}{\partial x^2} + \upsilon\frac{\partial^2 \phi_{mn}^{j}}{\partial y^2}\right)^2 (\phi_{mn}^{l})^2}{(\omega_{mn}^2 - \omega^2)^2 + (\beta_{mn}\omega)^2} S_{ff}(l,\omega)\,\mathrm{d}\omega, \tag{17}$$

$$\sigma_{My}^2(j,l) = \left(\frac{D^2}{2\pi}\right) \int_{-\infty}^{\infty} \sum_{m=1}^{\infty}\sum_{n=1}^{\infty} \frac{\left(\frac{\partial^2 \phi_{mn}^{j}}{\partial y^2} + \upsilon\frac{\partial^2 \phi_{mn}^{j}}{\partial x^2}\right)^2 (\phi_{mn}^{l})^2}{(\omega_{mn}^2 - \omega^2)^2 + (\beta_{mn}\omega)^2} S_{ff}(l,\omega)\,\mathrm{d}\omega, \tag{18}$$

$$\sigma_{Mxy}^2(j,l) = \left(\frac{1-\upsilon}{2}\right)^2 \left(\frac{D^2}{2\pi}\right) \int_{-\infty}^{\infty} \sum_{m=1}^{\infty}\sum_{n=1}^{\infty} \frac{\left(2\frac{\partial^2 \phi_{mn}^{j}}{\partial x \partial y}\right)^2 (\phi_{mn}^{l})^2}{(\omega_{mn}^2 - \omega^2)^2 + (\beta_{mn}\omega)^2} S_{ff}(l,\omega)\,\mathrm{d}\omega. \tag{19}$$

(b) MSV of CSD functions:

$$\sigma_{\kappa x}^2(j,l) = \frac{1}{2\pi} \int_{-\infty}^{\infty} \sum_{m=1}^{\infty}\sum_{n=1}^{\infty} \frac{\left(\frac{\partial^2 \phi_{mn}^{j}}{\partial x^2}\right)^2 (\phi_{mn}^{l})^2}{(\omega_{mn}^2 - \omega^2)^2 + (\beta_{mn}\omega)^2} S_{ff}(l,\omega)\,\mathrm{d}\omega, \tag{20}$$

$$\sigma_{\kappa y}^2(j,l) = \frac{1}{2\pi} \int_{-\infty}^{\infty} \sum_{m=1}^{\infty}\sum_{n=1}^{\infty} \frac{\left(\frac{\partial^2 \phi_{mn}^{j}}{\partial y^2}\right)^2 (\phi_{mn}^{l})^2}{(\omega_{mn}^2 - \omega^2)^2 + (\beta_{mn}\omega)^2} S_{ff}(l,\omega)\,\mathrm{d}\omega, \tag{21}$$

$$\sigma_{\kappa xy}^2(j,l) = \frac{1}{2\pi} \int_{-\infty}^{\infty} \sum_{m=1}^{\infty}\sum_{n=1}^{\infty} \frac{\left(2\frac{\partial^2 \phi_{mn}^{j}}{\partial x \partial y}\right)^2 (\phi_{mn}^{l})^2}{(\omega_{mn}^2 - \omega^2)^2 + (\beta_{mn}\omega)^2} S_{ff}(l,\omega)\,\mathrm{d}\omega. \tag{22}$$

Finally, the SSE for the undamaged plate due to bending and twisting MSDs is determined by substituting MSVs described in Eqs. (17)–(22) into Eq. (1), as follows:

$$\begin{aligned}\mathrm{SSE}^U = \left(\frac{D}{2\pi}\right)^2 \int_0^b \int_0^a \int_{-\infty}^{\infty} \Bigg\{ & \left[\sum_{m=1}^{\infty}\sum_{n=1}^{\infty}\left(\frac{\partial^2\phi_{mn}^j}{\partial x^2}+\upsilon\frac{\partial^2\phi_{mn}^j}{\partial y^2}\right)^2\left(\frac{\partial^2\phi_{mn}^j}{\partial x^2}\right)^2(\phi_{mn}^l)^4\right] \\ & + \left[\sum_{m=1}^{\infty}\sum_{n=1}^{\infty}\left(\frac{\partial^2\phi_{mn}^j}{\partial y^2}+\upsilon\frac{\partial^2\phi_{mn}^j}{\partial x^2}\right)^2\left(\frac{\partial^2\phi_{mn}^j}{\partial y^2}\right)^2(\phi_{mn}^l)^4\right] \\ & + \left[(2(1-\upsilon))^2\sum_{m=1}^{\infty}\sum_{n=1}^{\infty}\left(\frac{\partial^2\phi_{mn}^j}{\partial x\partial y}\right)^2\left(\frac{\partial^2\phi_{mn}^j}{\partial x\partial y}\right)^2(\phi_{mn}^l)^4\right]\Bigg\} \\ & \times\left\{\left(\frac{1}{\left(\omega_{mn}^2-\omega^2\right)^2+\left(\beta_{mn}\omega\right)^2}\right)^2\right\} S_{ff}^2(l,\omega)\,\mathrm{d}\omega\,\mathrm{d}x\,\mathrm{d}y, \end{aligned} \tag{23}$$

where SSE^U is SSE for the undamaged plate. Similarly, the SSE equation equivalent to Eq. (23) for undamaged beam-like structures can be obtained, as follows:

$$\mathrm{SSE}^U = \left(\frac{EI}{2\pi}\right)^2 \int_0^L \int_{-\infty}^{\infty} \left\{\sum_{m=1}^{\infty}\frac{\left(\frac{\partial^2\phi_m^j}{\partial x^2}\right)^2\left(\frac{\partial^2\phi_m^j}{\partial x^2}\right)^2(\phi_m^l)^4}{\left((\omega_m^2-\omega^2)^2+(2\zeta_m\omega_m\omega)^2\right)^2}\right\} S_{ff}^2(l,\omega)\,\mathrm{d}\omega\,\mathrm{d}x. \tag{24}$$

The SSE for different damage conditions, SSE^D, can also be analogously defined.

Finally, some of the advantages of the SSE approach for structural damage identification are summarized below: bending/twisting MSDs are related to realistic load-resisting behaviour of structures and characterize its response behaviour; broadband frequency information is utilized unlike its alternative counterparts, namely MSE where only resonance frequency information is used; multiple response parameters (i.e., mode shapes, natural frequencies and modal damping) are employed; sensitivity of the response parameters to damage can be increased by considering a less noisy band of response MSD and CSD or bandwidth-localized strain energy in terms of spectral moments; and the approach can be used for output-only damage identification problems with the assumption that the excitation force is stationary, ergodic white noise.

3. Damage identification methods

In this study, SSE values computed for different structural conditions (i.e., undamaged and damaged states) are used in the corresponding damage identification algorithms to detect and localize simulated damage. The damage/performance indices that are used in this study include RRMSE and normalized damage index. The following assumptions and steps are used for computation of MSD, CSD, SSE and damage indices: (i) the excitation force is assumed to be a stationary ergodic random process; (ii) the effects of internal damage are most apparent in a local reduction of stiffness, simulated here by reducing the values of Young's modulus at selected elements in the FE model. Modal parameters for undamaged and damaged states are obtained using ANSYS 8.0 [23] for single and multiple damage conditions; (iii) the influence damping on the overall accuracy of the proposed global damage identification method is considered to be not critical as long as lower frequency vibration modes are employed. For well-separated lower modal frequencies, changes in the damping properties due to damage are assumed to be consistent across modes; (iv) displacement response functions at simulated measurement grid points are generated using the normal mode analysis method. Consequently, MSD, CSD and the respective MSVs are computed at each grid point; (v) SSEs are computed for different damage conditions by using MSVs; and (vi) damage identification is conducted using various damage indices and the results are compared graphically with those obtained from an existing damage identification method, namely MSE. Finally, for computation of damage indices the argument used by Cornwell et al. [8] is adopted,

where the fractional energy and bending stiffness of the plate are assumed to remain constant for both undamaged and damaged sub-regions and over the whole area of the plate.

3.1. Damage index using normalized SSE

The SSE damage indices are computed using the ratio of an element-based SSE for the damaged state to the undamaged state determined for each element using Eq. (25). These indices are then normalized against their statistical mean value from which damage localization is conducted using a statistical hypothesis test [8]:

$$\mathrm{DI}^{e}=\frac{\mathrm{SSE}^{D_e}/(\mathrm{SSE}^{D})_{\mathrm{mean}}}{\mathrm{SSE}^{U_e}/\left(\mathrm{SSE}^{U}\right)_{\mathrm{mean}}}=\frac{\dfrac{1}{L}\sum_{j=1}^{L}\mathrm{SSE}_{j}^{D_e}\Big/\dfrac{1}{n_e}\sum_{e=1}^{n_e}\mathrm{SSE}^{D_e}}{\dfrac{1}{L}\sum_{j=1}^{L}\mathrm{SSE}_{j}^{U_e}\Big/\dfrac{1}{n_e}\sum_{e=1}^{n_e}\mathrm{SSE}^{U_e}}, \tag{25}$$

where DI^{e} is the element-based damage index; SSE^{U_e} and SSE^{D_e} are SSE for undamaged and damaged plate element e, respectively. L is the number of nodes for each element and n_e is the total number of elements used in the model. By introducing the mean μ_{DI} and standard deviation σ_{DI} of the damage indices, only those peaks satisfying the following condition are believed to be associated with damage locations:

$$Z^{e}=\frac{\mathrm{DI}^{e}-\mu_{\mathrm{DI}}}{\sigma_{\mathrm{DI}}}\geqslant C_r, \tag{26}$$

where $\mu_{\mathrm{DI}}=(1/n_e)\sum_{e=1}^{n_e}\mathrm{DI}^{e}$ and $\sigma_{\mathrm{DI}}=\sqrt{(n_e\sum(\mathrm{DI}^{e})^2(\sum\mathrm{DI}^{e})^2)/n_e(n_e-1)}$. Z^{e} is the normalized damage index for element e and C_r is the critical value. The damage threshold is established from C_r the value which is associated with the level of significance used for the hypothesis test.

3.2. Damage index using relative RMS error

Damage indices which are implemented based on an error characterization technique known as RRMSE, are then used for assessment of percentage changes in the response parameters due to different levels of damage and to localize damage, as follows:

$$\mathrm{DI}^{e}(\mathrm{RRMSE})=\left(\frac{\dfrac{1}{L}\sum_{j=1}^{L}(\mathrm{SSE}_{j}^{D_e}-\mathrm{SSE}_{j}^{U_e})^{2}}{\dfrac{1}{L}\sum_{j=1}^{L}(\mathrm{SSE}_{j}^{U_e})^{2}}\right)^{1/2}, \tag{27}$$

where $\mathrm{DI}^{e}(\mathrm{RRMSE})$ is the element-based damage index. $\mathrm{SSE}_{j}^{D_e}$ and $\mathrm{SSE}_{j}^{U_e}$ are the spectral strain energies at point j and element e of the damaged and undamaged states, respectively.

4. Numerical analysis studies

To illustrate the effectiveness of the proposed method, a simply supported rectangular reinforced concrete plate and a beam structure are considered for damage identification of single and multiple simulated damage conditions. The material properties for the undamaged plate include Young's modulus of 20 GPa, mass density of 2400 kg/m^3 and Poisson's ratio of 0.25, Similarly, a Young's modulus of 30 GPa, mass density of 2400 kg/m^3 and Poisson's ratio of 0.25 is used for the beam element.

The finite element (FE) model of the plate consists of 16×24 elements meshed with SHELL63 (Fig. 1) and the beam consists of 50 elements meshed with the BEAM3 of ANSYS 8.0 (Fig. 2). Damage is assumed to alter only the stiffness properties and is simulated by reducing the Young's modulus at pre-determined element locations. The level of damage severity applied is directly related to the percent reduction adopted for the Young's modulus. The following two types of damage cases are considered in this study: (i) single damage is

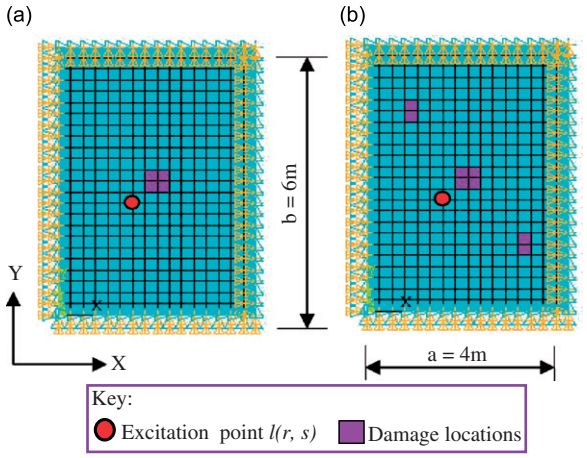

Fig. 1. Finite element model for simply supported rectangular plate with measurement grid points and damage locations indicated: (a) single damage and (b) multiple damages.

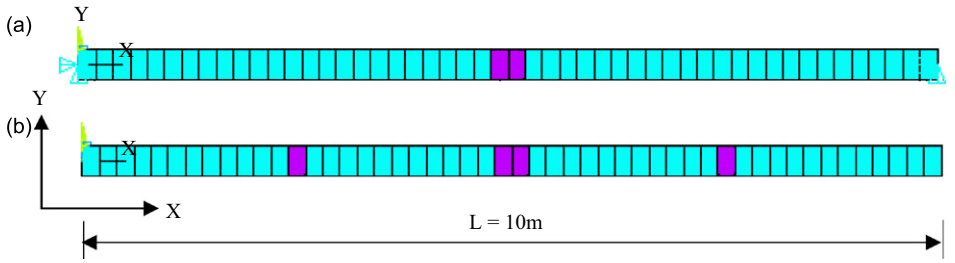

Fig. 2. Finite element model for simply supported beam with measurement grid points and damage locations indicated: (a) single damage and (b) multiple damages.

induced at the centre of the plate (Fig. 1a) with 5%, 10% and 20% severity levels while 5%, 10%, 15% and 20% damage levels are applied at the mid-span of the beam (Fig. 2a); (ii) multiple damages are induced at three locations (Figs. 1b and 2b) with the same levels of damage severity as case (i) for respective plate and beam elements. Therefore, the changes in the Young's modulus due to the induced damage to the plate structure becomes 1, 2 and 4 GPa for 5%, 10% and 20% damage severity levels, respectively. Similarly, for the case of the damaged beam, the changes in the Young's modulus include 1.5, 3, 4.5 and 6 GPa for 5%, 10%, 15% and 20% damage severity levels, respectively.

In addition, different levels of damage severity were simultaneously applied to plate and beam structural elements (i.e., 5%, 10% and 20% for the plate and 10%, 15% and 20% for the beam element). For each damage state, modal frequencies and the mode shapes are determined from FE-based modal analysis. A constant damping ratio of 1% and a frequency resolution of 0.0625 Hz were adopted for generation of the response parameters in the frequency domain. The modal parameters obtained for the first 10 modes are used to generate MSD, CSD, MSV, SSE and MSE. Consequently, the damage indices are computed using each response parameter and damage identification studies are subsequently conducted. Finally, the identification results are presented graphically for both single and multiple simulated damage states and for both structural elements (Figs. 3–12).

4.1. Discussion on damage identification results

Damage identification results for the single and multiple damage cases under study using different techniques are presented in Figs. 3–12. Fig. 3 shows a typical response SSE integrand for the reinforced concrete plate element where shifts in the resonance frequencies are used for assessment of structural damage.

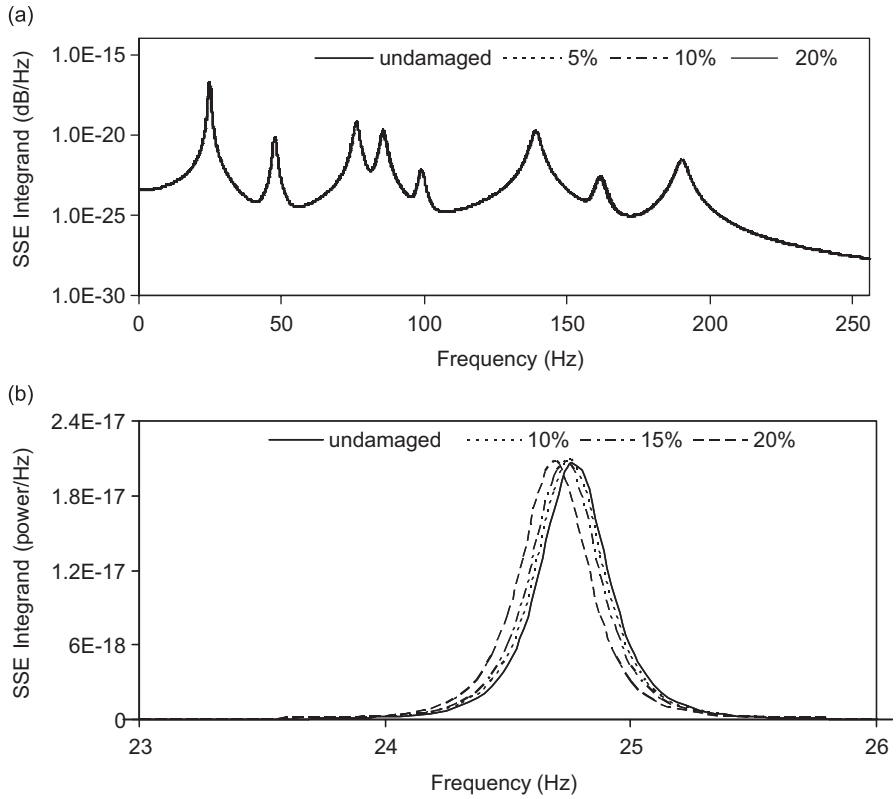

Fig. 3. Damage assessment in plate element using typical integrand of response SSE: (a) plot for the full-frequency range and (b) magnified plot (for the first mode).

However, these shifts were found to be too small to indicate any changes or to be usable for identification of structural damage. The maximum frequency changes observed are about 0.6% for 20% damage severity and only 0.2% for 5% damage severity. Similar results were also observed for the structural beam element. This indicates that for massive civil structures such as concrete structures, where localized damage is experienced, natural frequencies are not the best candidates as indicators of changes in structural condition. Therefore, the damage identification indices presented in Section 3 are used to localize damage and to compare the performance of the SSE method and the MSE method.

4.1.1. Damage identification results using normalized SSE

Figs. 4–7 show the capability of the SSE method for identification of damage in plate and beam elements. Both single and multiple damage conditions are detected and localized using a normalized damage index technique. The results show that the peak values of the damage indices are observed at the exact damage locations pre-determined from the numerical model and using a C_r value of 2 corresponding to a 95% confidence bound, (see Figs. 4–7). However, in the case of a differential variation of damage severity across the plate element ranging from 5% to 20%, the C_r value of 1.28 corresponding to 90% confidence level is adopted in order to accurately localize all the damages (Fig. 5d). In general, the SSE-based normalized damage index method clearly indicates the exact location of damage that has been artificially introduced to both the plate and beam elements.

4.1.2. Damage identification results using RRMSE

The RRMSE is used as a performance index in order to demonstrate that SSE provides more sensitive response parameters that perform better than existing counterparts. Damage identification results for both

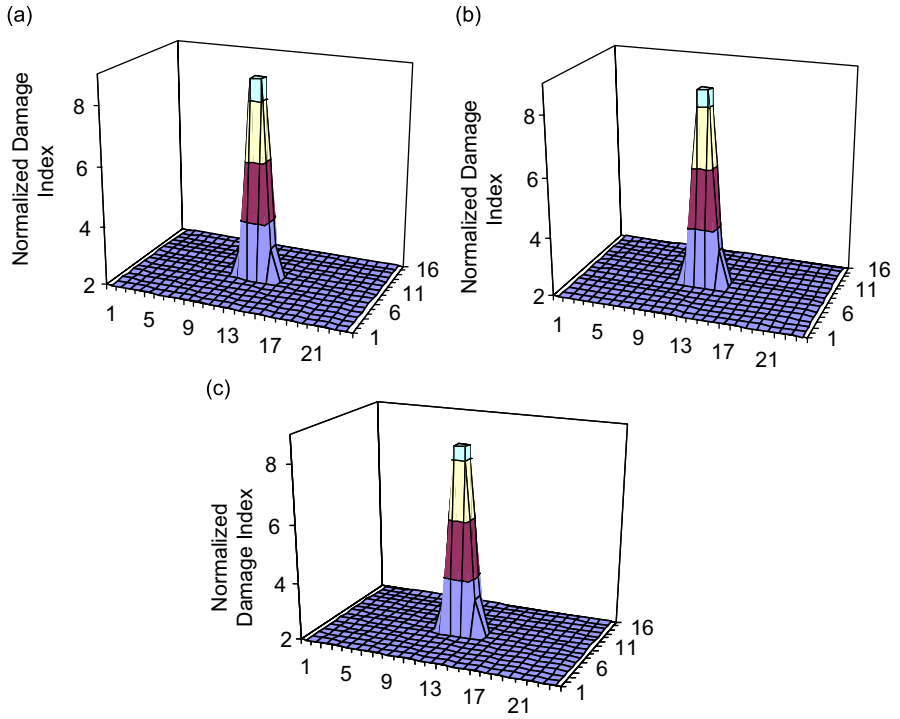

Fig. 4. Single damage identification in plate element using normalized SSE: (a) 20% damage, (b) 10% damage and (c) 5% damage.

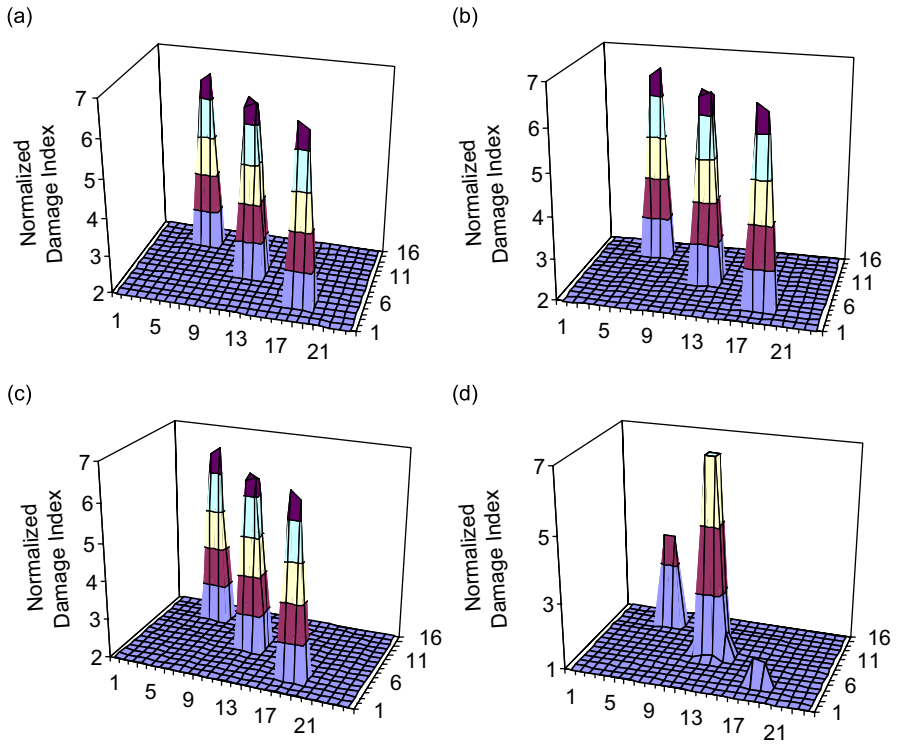

Fig. 5. Multiple damage identification in plate element using normalized SSE: (a) 20% damage, (b) 10% damage, (c) 5% damage and (d) 5_10_20% damage.

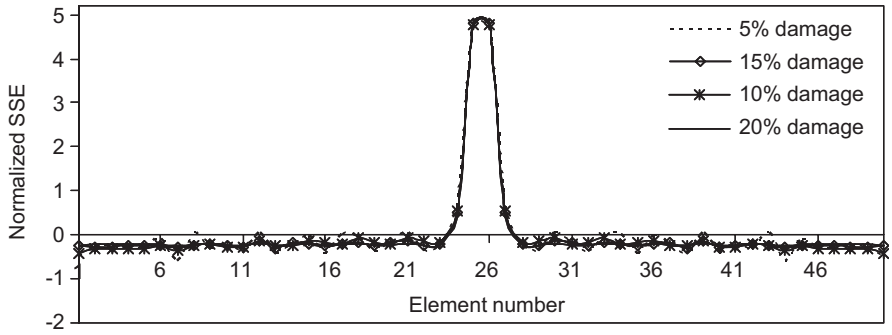

Fig. 6. Single damage identification in beam element using normalized SSE.

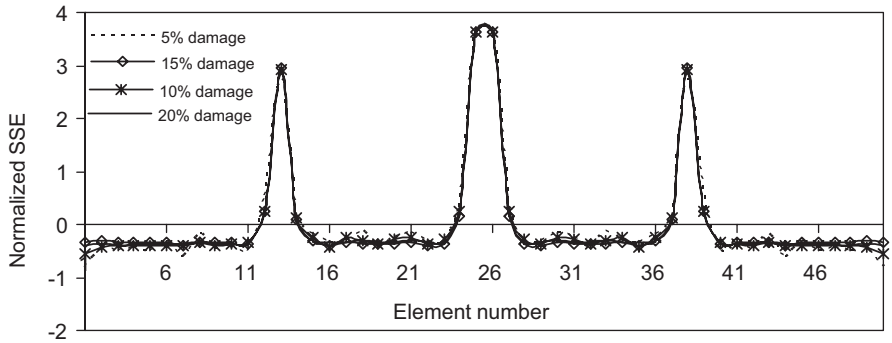

Fig. 7. Multiple damage identification in beam element using normalized SSE.

SSE and MSE by using RRMSE-based performance index are presented for both plate and beam elements, (see Figs. 8.1–12). The results obtained using RRMSE values indicate existence, location and relative severity of damage in both plate and beam structural elements. Both single and multiple damage conditions are identified effectively using RRMSE obtained from SSE and MSE. However, performance or sensitivity levels of these two parameters are found to be significantly different.

Comparisons of their damage identification capabilities are conducted based on the maximum changes in RRMSE values of SSE and MSE for different damage levels, as follows: (i) For the plate damage case, the maximum changes observed in RRMSE of SSE for the single as well as multiple damage cases are about three times that of MSE (Figs. 8.1–9.4). (ii) For the beam damage case, the changes observed in RRMSE of SSE for the single damage case is about four times that of MSE (Fig. 10), about five times for multiple damage case (Fig. 11), and four times for differential multiple damage case (Fig. 12). Finally, it can be concluded that SSE is much more sensitive to damage than the existing and now well established method known as MSE. This is primarily due to the use of broadband information in the case of SSE which is lacking in the case of MSE since this latter method is based on resonance frequency information.

4.2. Damage identification using noisy response data

In practice, real measurement data is always liable to contamination with the inevitable presence of random noise. Therefore, it is necessary to examine the performance of the proposed method in the presence of random noise by considering pollution of the numerically obtained response data. Therefore, the time-domain response time histories obtained at each grid points are polluted with spatially random noise, with mean zero, variance one and standard deviation one, as follows:

$$A_{kN}(t) = A_{k0}(t)\left(1 + \frac{e}{100} \times \text{randn}(m,n,p)\right), \tag{28}$$

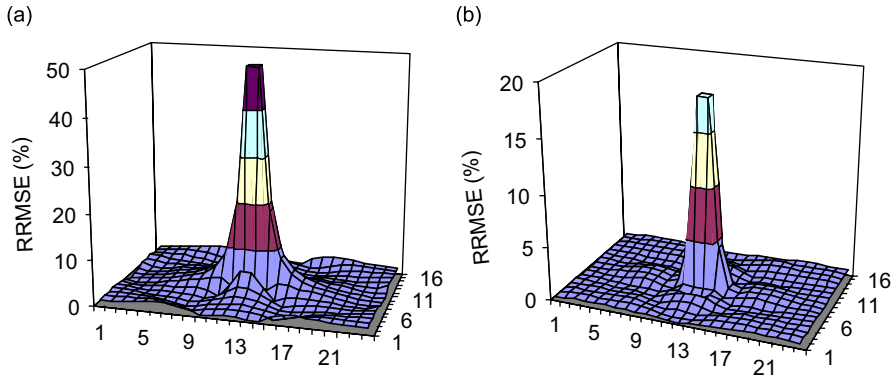

Fig. 8.1. Single damage identification in plate element using relative root mean-square error (RRMSE) for 20% damage: (a) SSE and (b) MSE.

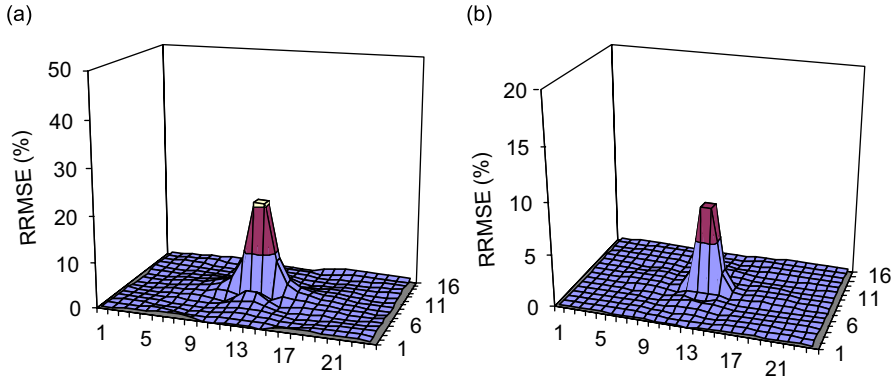

Fig. 8.2. Single damage identification in plate element using relative root mean-square error (RRMSE) for 10% damage: (a) SSE and (b) MSE.

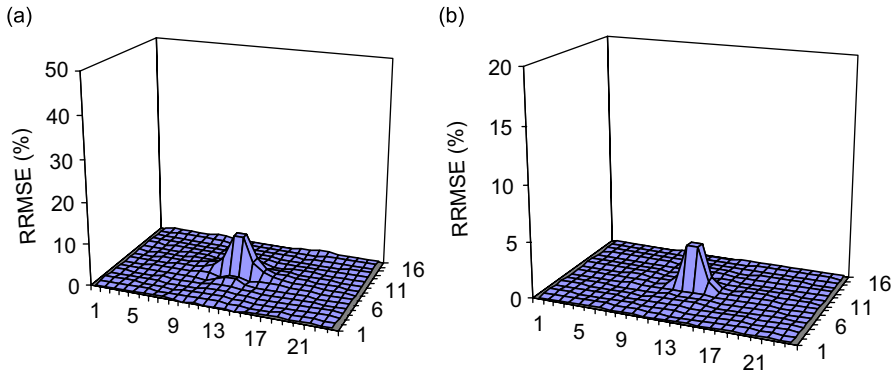

Fig. 8.3. Single damage identification in plate element using relative root mean-square error (RRMSE) for 5% damage: (a) SSE and (b) MSE.

where A_{k0} is the noise free responses at grid point k and A_{kN} is the corresponding noise polluted response, randn is a MATLAB® function used for generation of random noise for different damage conditions, m is the size of the samples in the time series, n the number of measurement grid points, p the size of the repeat test data used for the ensemble average ($p = 10$) and e the level of noise in percent.

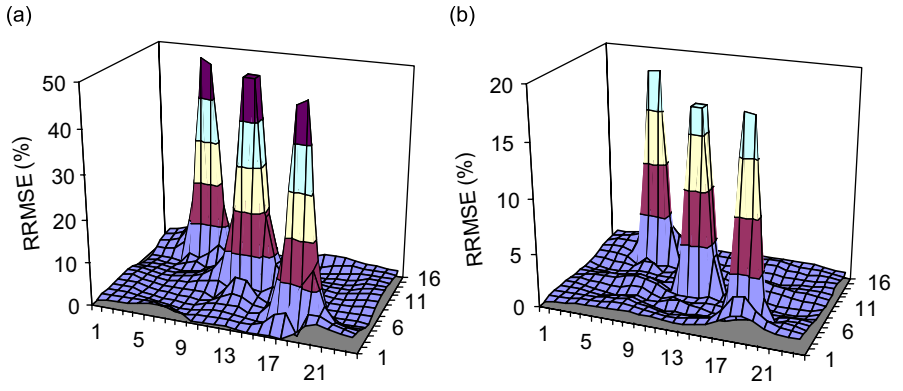

Fig. 9.1. Multiple damage identification in plate element using relative root mean-square error (RRMSE) for 20% damage: (a) SSE and (b) MSE.

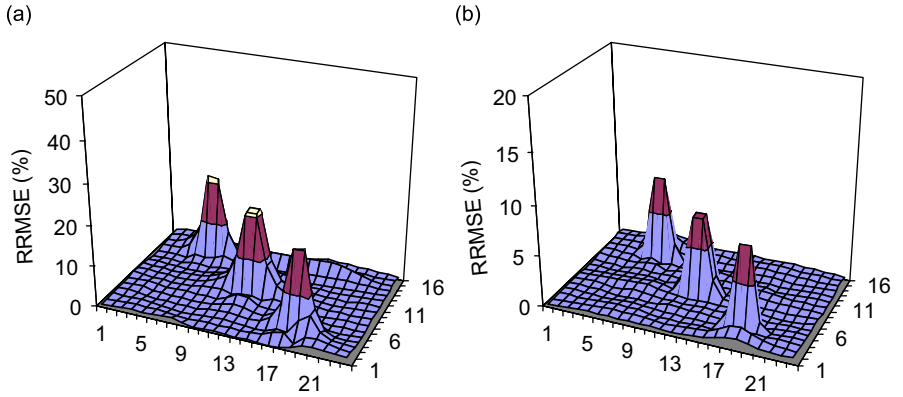

Fig. 9.2. Multiple damage identification in plate element using relative root mean-square error (RRMSE) for 10% damage: (a) SSE and (b) MSE.

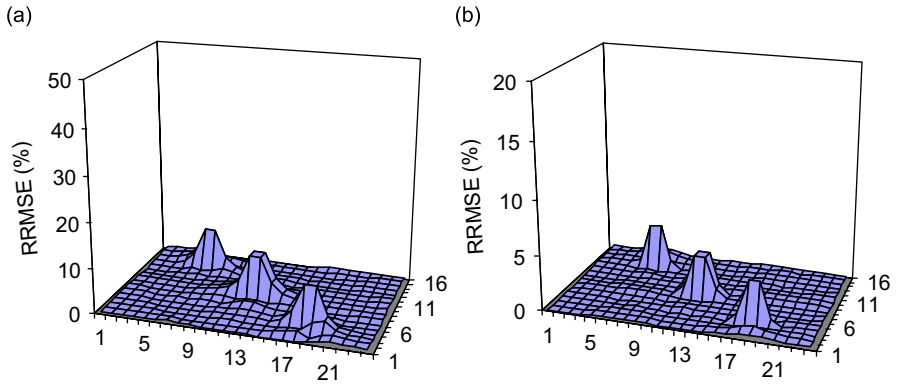

Fig. 9.3. Multiple damage identification in plate element using relative root mean-square error (RRMSE) for 5% damage: (a) SSE and (b) MSE.

The general procedures involved in the analysis can be described as follows. First, a linear time history analysis is conducted on the plate model to obtain noise-free responses. A broadband excitation simulated by using impact load with duration of a single integration time step (ITS) is used to determine the response time

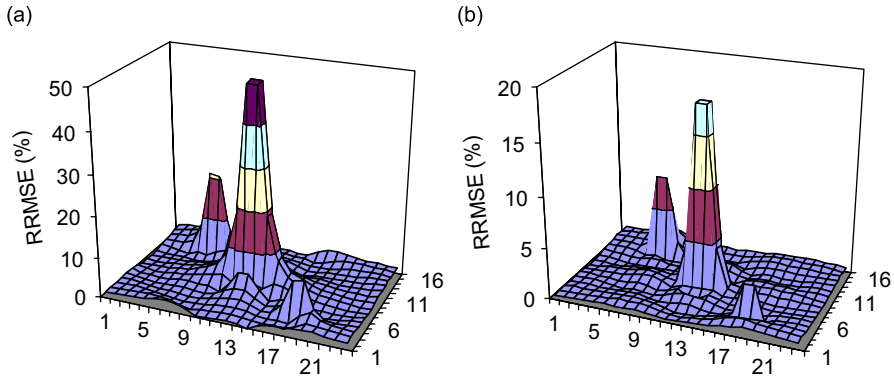

Fig. 9.4. Multiple damage identification in plate element using relative root mean-square error (RRMSE) for 5_10_20% damage: (a) SSE and (b) MSE.

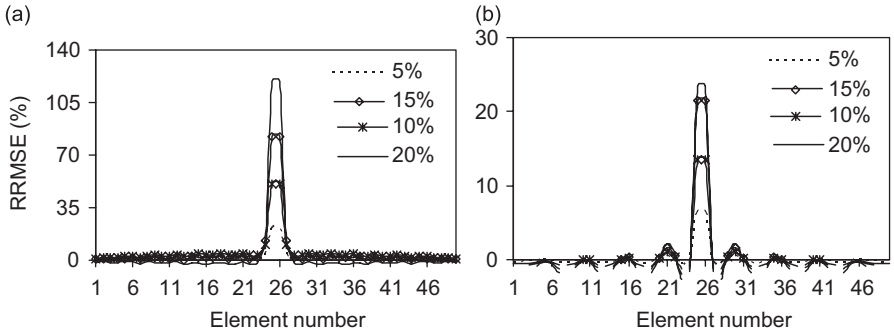

Fig. 10. Comparison of damage identification methods based on RRMSE values and for different level of single damage in beam element: (a) SSE and (b) MSE.

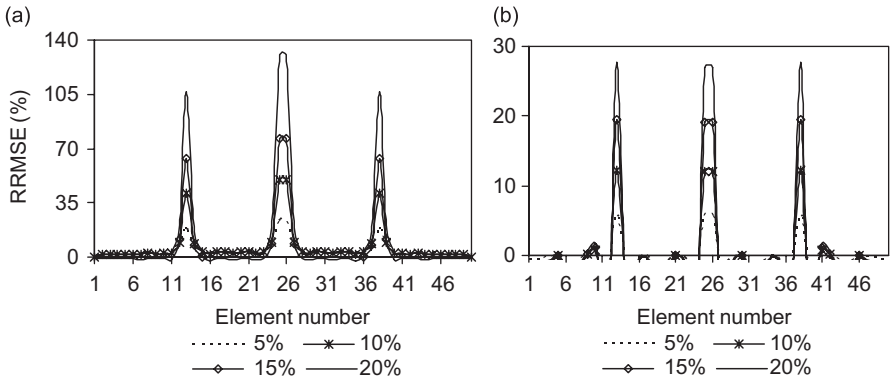

Fig. 11. Comparison of damage identification methods based on RRMSE values and different level of multiple damages in beam element: (a) SSE and (b) MSE.

history using ANSYS. A sampling period of 8 s, ITS values of 0.00024414 s and sampling frequency of 4096 Hz are employed to obtain 32,768 samples of noise-free responses at each grid point. Secondly, the responses thus obtained are polluted with spatially random noise, where 5% and 10% noise levels ($e = 5\%$ and 10%) are applied. Third, the FFT is then conducted on the noise polluted repeat data at each grid point and ensemble

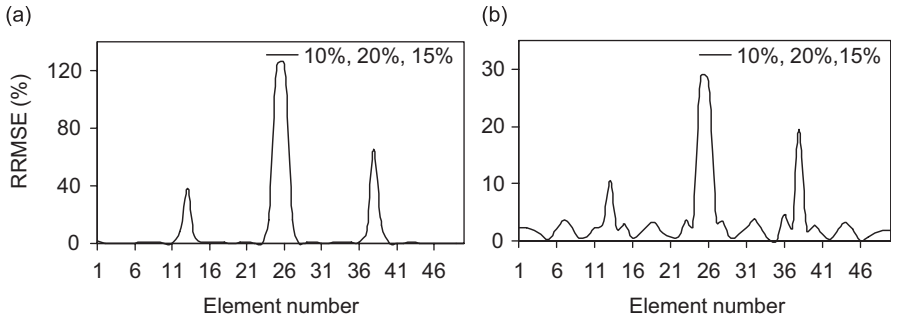

Fig. 12. Comparison of damage identification methods based on RRMSE values and different level of multiple differential damages in beam element: (a) SSE and (b) MSE.

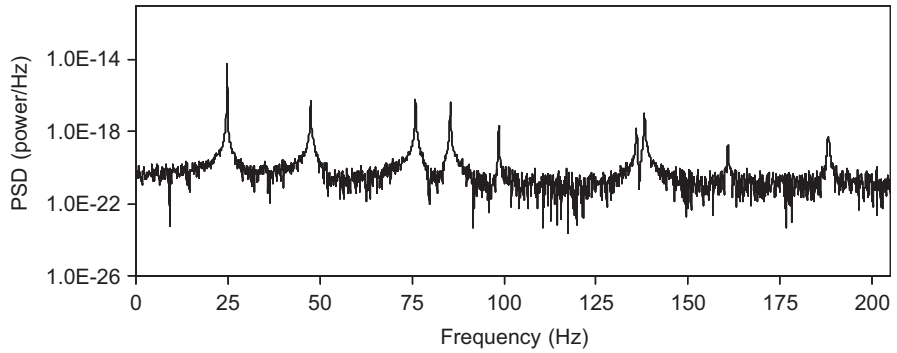

Fig. 13. The vibration response PSD for a typical grid point with 10% noise pollution.

averaging is performed in the frequency domain. Ensemble average techniques are normally used in random signal analysis in order to determine the overall frequency content of the signal and to reduce noise and high-frequency content. The response PSD at a typical grid point considering 10% random noise is shown in Fig. 13. Fourth, an inverse FFT is conducted on the ensemble averaged frequency domain response data to obtain time-domain data. Finally, experimental modal analysis is conducted on the time-domain data using the natural input modal analysis software from Structural Vibration Solutions, A/S [24]. The peak picking modal identification method implemented in the frequency domain decomposition option of the ARTeMIS Extractor® software is employed to determine the natural frequencies and mode shapes for the first 10 modes. (The trial version of the software does not provide options for estimation of modal damping and is a less accurate version of the ARTeMIS Extractor® software.) Finally, both SSE and MSE are constructed and damage identification studies are conducted. However, the damage identification results obtained using only the significant percentage of random noise (10%) and the normalized damage index method are presented (Figs. 14 and 15).

4.2.1. Discussion on damage identification results of the noisy response data

In general, the capability of the proposed damage identification method is found to be dependent on the level of noise pollution and the type of damage classification index used. At the same time, the SSE method is able to localize all the damage conditions, single as well as multiple damage cases, despite the presence of 10% random noise and the use of a less accurate modal analysis tool (Figs. 14(a)–(c) and 15(a)–(c)). For less severe damage conditions some false positive damage identifications are observed near the plate boundaries. This is because of the combined influence of noise and the susceptibility of Eq. (25) to numerical instability when numerator and denominator are close to zero. This occurs when the responses determined close to the supports of the plate are relatively small. On the other hand, the existing method (MSE) is able to correctly

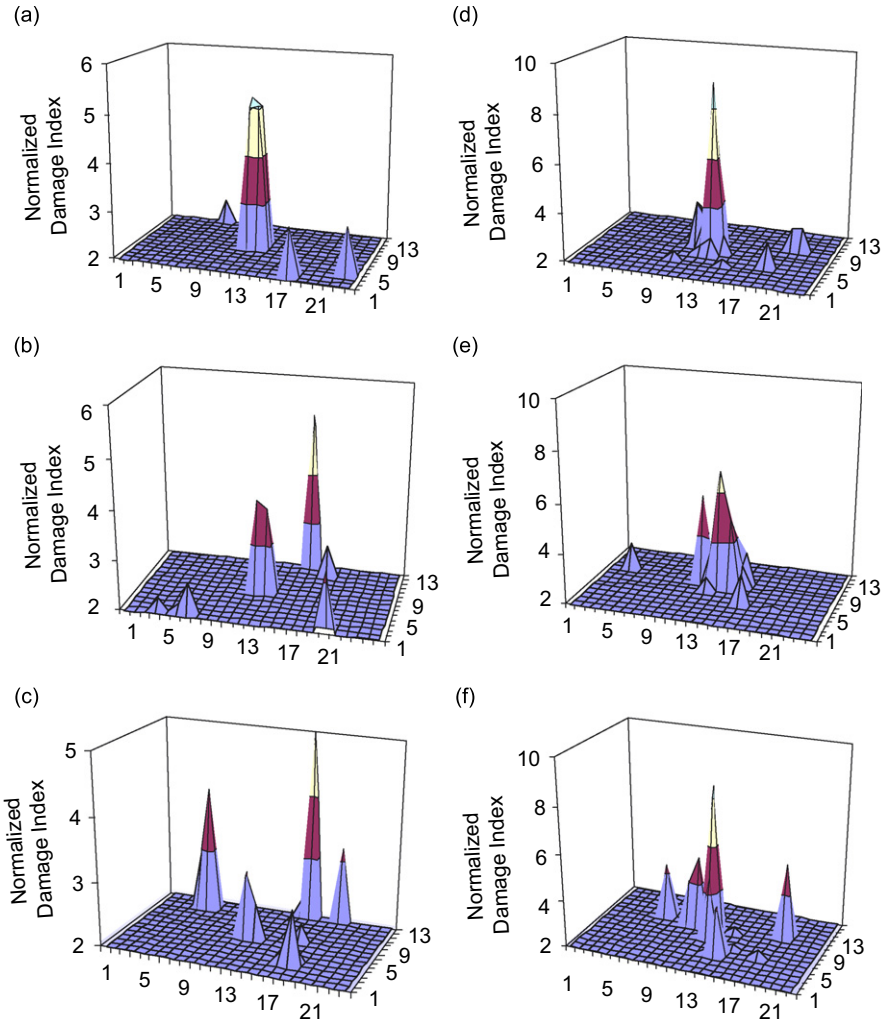

Fig. 14. Single damage identification in plate element using 10% random noise polluted modal data, (i) normalized SSE: (a) 20% damage, (b) 10% damage, (c) 5% damage; and (ii) normalized MSE: (d) 20% damage, (e) 10% damage, (f) 5% damage.

localize only the single damage cases with severe levels of damage (Figs. 14(d)–(f)). However, the MSE method was not able to effectively localize multiple damage conditions (Fig. 15(d)–(f)). Therefore, these results confirm that the proposed SSE method can outperform the existing MSE method in the presence of significant levels of noise. Overall, it can be said that the proposed SSE method is resistant to measurement noise and modal identification error.

4.3. Damage identification using incomplete and noisy response data

In this section, the robustness of the proposed SSE method is assessed by considering the combined influence of practical scenarios inevitable in real-world applications. These scenarios include an incomplete number of measurement grid points, limited number of modes and noise-corrupted data. The statistics used for this investigation include: data at 13-by-9 grid points as compared to 25×17 grids (or one-fourth of the initial number of elements used for damage identification studies conducted in the preceding sections) which are subsets of the original data and determined at every second point across each grid line; the first five flexural

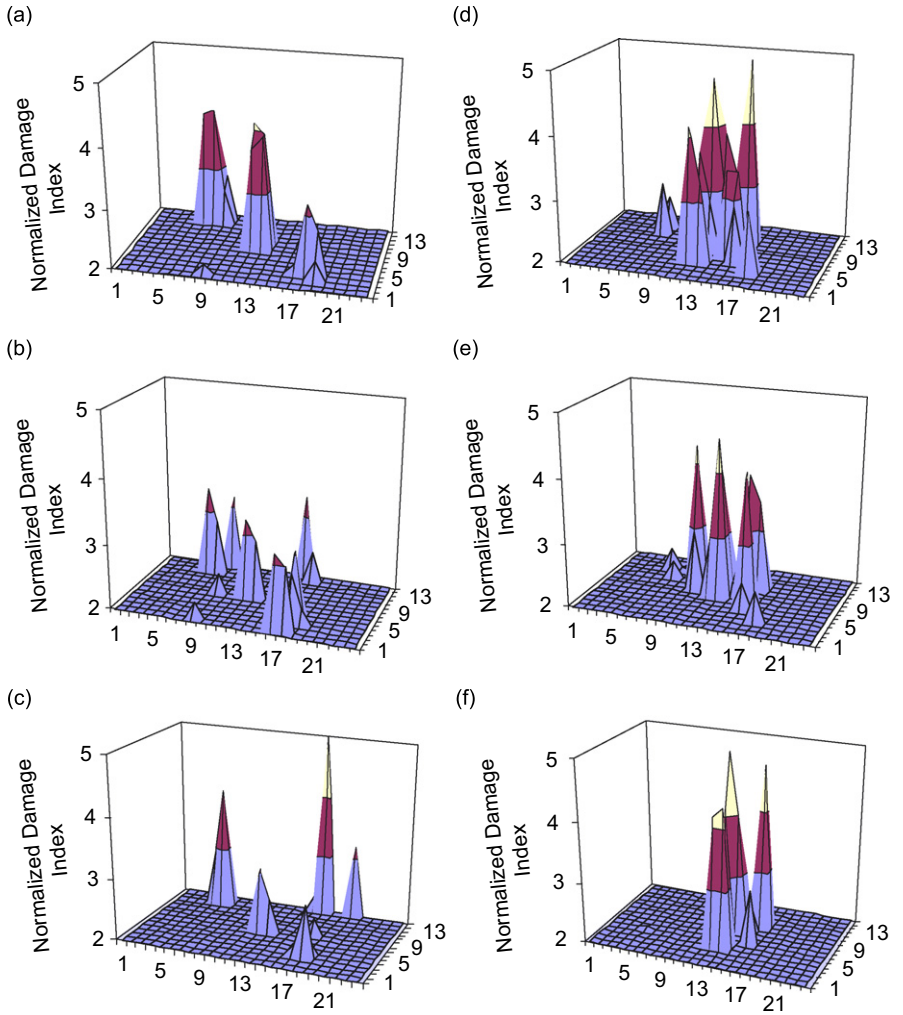

Fig. 15. Multiple damage identification in plate element using 10% random noise polluted modal data, (i) normalized SSE: (a) 20% damage, (b) 10% damage, (c) 5% damage; and (ii) normalized MSE: (d) 20% damage, (e) 10% damage, (f) 5% damage.

modes (or half of the number of modes used in the preceding sections); and 10% random noise level. The results obtained using the normalized SSE and MSE methods are presented in Figs. 16 and 17.

4.3.1. Discussion on damage identification results of the incomplete and noisy response data

The results indicate that both the SSE and MSE methods are able to effectively localize single damage conditions of various severities despite the use of sparse and noisy response data (Fig. 16(a)–(f)). However, in the case of multiple damage conditions, the SSE method is found to be more accurate in localizing all the damage than the MSE method, as shown in Figs. 17(a)–(c) and 17(d)–(f)), respectively. For instance, the MSE method is not able to correctly localize all of the damage for 5% damage severity (Fig. 17(f)). Overall, the accuracy of the damage identification results for both SSE and MSE were seen to be increased as compared to those presented in Section 4.2 despite the significant reduction in measurement grid points and flexural modes. The possible reasons are attributed to: first, the increased size of grid elements are expected to minimize the numerical instability caused by the ratio of two small numbers near the plate boundaries. Secondly, the lower flexural modes are often determined more accurately from experimental modal analysis than the higher modes and therefore may have assisted in an increased accuracy for both SSE and MSE methods. Finally, the overall

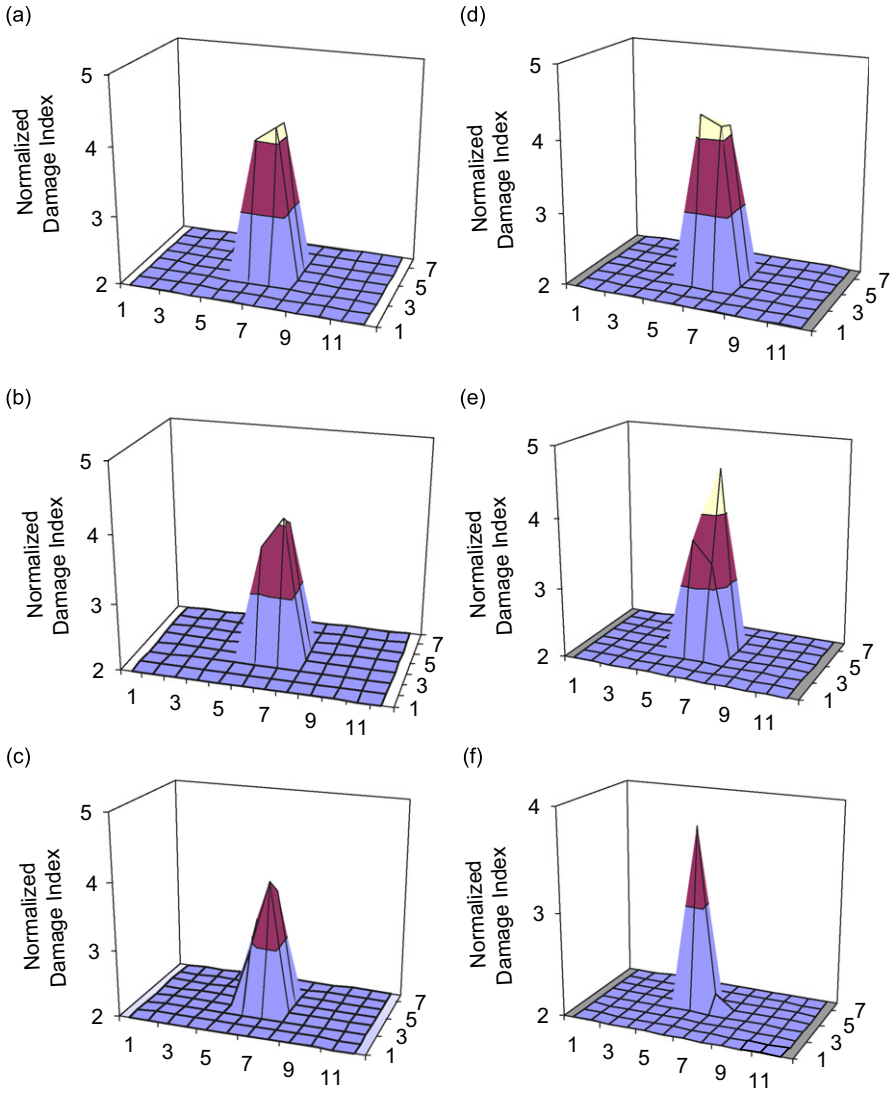

Fig. 16. Single damage identification in plate element using 10% random noise polluted and sparse modal data, (i) normalized SSE: (a) 20% damage, (b) 10% damage, (c) 5% damage; and (ii) normalized MSE: (d) 20% damage, (e) 10% damage, (f) 5% damage.

results strongly confirm that the SSE method consistently outperformed the MSE method in the presence of measurement noise, incomplete modal data, incomplete number of modes and modal identification error. Moreover, the results also indicate that sparse modal data and measurement noise are more likely to influence the performance of MSE than the proposed SSE method.

5. Experimental verification study

In the preceding sections, the superior performance of the proposed SSE damage identification method over the MSE was demonstrated using extensive numerical simulation studies. In this section, the performance and robustness of the SSE parameter is verified with experimental modal data (namely resonance frequencies, mode shapes and modal damping) from the I-40 Bridge subjected to various damage conditions. Descriptions of the damage scenarios induced at the mid-point of the middle span of the north plate-girder of the I-40 Bridge during the modal testing include: (i) damage scenario E-1: consisted of a 61 cm long and 0.95 cm wide cut through the web centred at the mid-height of the web; (ii) damage scenario E-2: extension of the damage

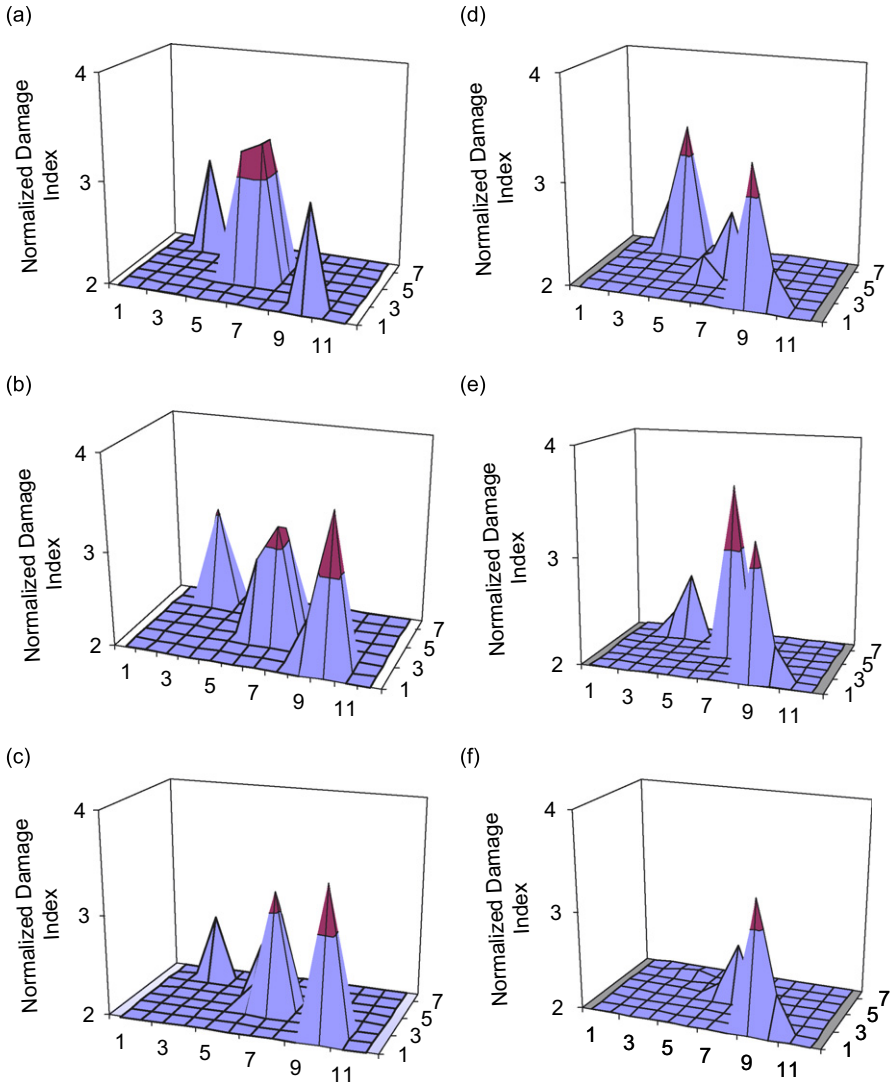

Fig. 17. Multiple damage identification in plate element using 10% random noise pollution and sparse modal data, (i) normalized SSE: (a) 20% damage, (b) 10% damage, (c) 5% damage; and (ii) normalized MSE: (d) 20% damage, (e) 10% damage, (f) 5% damage.

scenario E-1 up to the bottom flange—an approximately 183 cm to long cut; (iii) damage scenario E-3: extension of 183 cm long cut in the web to halfway into the bottom flange towards either side; and (iv) damage scenario E-4: consisted of the 183 cm long cut in the web extended through the entire bottom flange. Detailed information regarding the I-40 Bridge, experimental procedures and damage identification studies conducted on this bridge can be found elsewhere [25–28].

Two types of vibration tests were conducted for measurement of modal properties of the I-40 Bridge: a forced vibration test and ambient vibration tests. In this paper, the modal data from the forced vibration test is used for verification of input–output damage identification while the modal data from ambient vibration tests is employed for verification of output-only damage identification capability of the proposed SSE parameter. The forced vibration test was conducted on the whole portion of the bridge using a hydraulic shaker to generate measured input force to the bridge. Consequently, a coarse set of measurement grid points was used for acceleration response measurements in the two plate girders using 26 accelerometers. The number of accelerometers actually mounted on the span of the north plate girder where damage was induced was 13

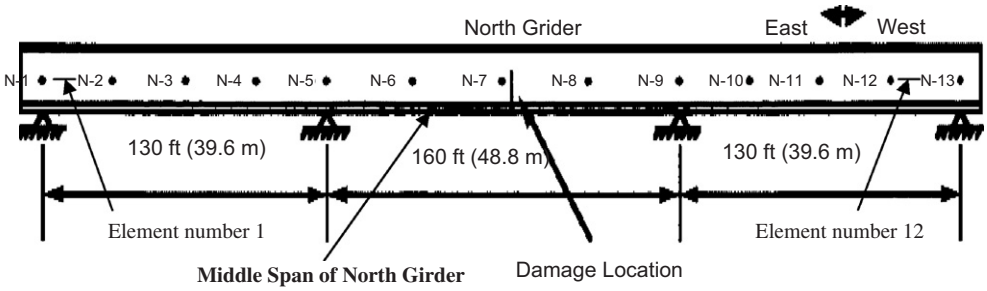

Fig. 18. Locations of the coarse set of accelerometers (SET1) on the north plate girder during forced vibration test with location of damage indicated.

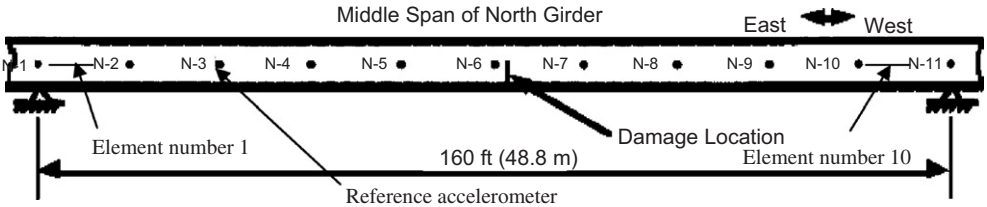

Fig. 19. Location of the refined set of accelerometers (SET2) on the middle span of the north plate girder during ambient vibration testing of the I-40 Bridge.

(Fig. 18). The measurement data sets obtained from this test for different damage condition states was referred to as SET1. Finally, modal frequencies, mode shapes and modal damping ratios for the first six modes were extracted from the FRFs of SET1 measurement data [25,29]. Moreover, unit-mass normalized mode shapes were obtained since the input force and the driving point acceleration were measured.

Similarly, ambient vibration testing was conducted using a refined set of accelerometers (SET2) on the middle span of the north plate girder of the bridge portion tested (Fig. 19). The acceleration response measurements were made for both undamaged and damaged conditions while a random input excitation from a shaker was applied. Finally, the modal parameters were extracted from amplitude and phase information of the cross-power spectra of the SET2 measurements relative to accelerometer reading at reference grid point N-3. The modal parameter results for the first three modes can be found from the references provided [25,28,29]. Since the random excitation force input was not measured for this test, unit-mass normalized mode shapes cannot be obtained. Hence, mode shape vectors were consistently normalized using an identity mass matrix.

5.1. Damage localization results in I-40 Bridge

For the verification studies conducted, only the first two vibration modes of the I-40 Bridge were employed. This is because the results from the previous studies indicated that the use of all the identified modes for damage identification did not significantly improve the accuracy of the results. Moreover, damage scenarios E-1 and E-2 were not considered for this verification study. This decision was taken based on the observation that the modal frequencies of these two cases were found to marginally increase relative to those frequencies obtained from the undamaged condition of the bridge. The reason suggested in the literature referenced is the changing test conditions and low level of damage [27]. Cubic polynomial and spline interpolation methods were employed to determine mode shapes at a refined set of grid points between sensors. To overcome numerical instability due to small response amplitude near support conditions, appropriate measures were applied to the SSE parameter. These include division by their norm and shifting of the reference coordinate SSE parameter vectors by 1 prior to computation of the damage indices. Therefore, the element-based damage

index given in Eq. (25) is modified in the form

$$\mathrm{DI}^{e}=\frac{\left(\dfrac{\mathrm{SSE}^{D_e}}{\|\mathrm{SSE}^{D_e}\|}\Big/\dfrac{(\mathrm{SSE}^{D})_{\mathrm{mean}}}{\|(\mathrm{SSE}^{D})_{\mathrm{mean}}\|}\right)+1}{\left(\dfrac{\mathrm{SSE}^{U_e}}{\|\mathrm{SSE}^{U_e}\|}\Big/\dfrac{(\mathrm{SSE}^{U})_{\mathrm{mean}}}{\|(\mathrm{SSE}^{U})_{\mathrm{mean}}\|}\right)+1}=\frac{\left(\dfrac{\dfrac{1}{L}\sum_{j=1}^{L}\mathrm{SSE}_j^{D_e}}{\left\|\dfrac{1}{L}\sum_{j=1}^{L}\mathrm{SSE}_j^{D_e}\right\|}\Big/\dfrac{\dfrac{1}{ne}\sum_{e=1}^{n_e}\mathrm{SSE}^{D_e}}{\left\|\dfrac{1}{n_e}\sum_{e=1}^{n_e}\mathrm{SSE}^{D_e}\right\|}\right)+1}{\left(\dfrac{\dfrac{1}{L}\sum_{j=1}^{L}\mathrm{SSE}_j^{U_e}}{\left\|\dfrac{1}{L}\sum_{j=1}^{L}\mathrm{SSE}_j^{U_e}\right\|}\Big/\dfrac{\dfrac{1}{n_e}\sum_{e=1}^{n_e}\mathrm{SSE}^{U_e}}{\left\|\dfrac{1}{n_e}\sum_{e=1}^{n_e}\mathrm{SSE}^{U_e}\right\|}\right)+1}. \tag{29}$$

5.2. Discussion on damage identification results of the verification study

Damage localization results of the SSE method obtained in terms of normalized DI are presented for SET1 and SET2 in Figs. 20(a, b) and 21(a, b), respectively. From the observation of the values of the normalized DI greater or equal to 2, it can be concluded that SSE is able to localize both damage scenarios (E-3 and E-4) using coarse (SET1) as well as refined (SET2) measurement data, as shown in Figs. 20(a, b) and 21(a, b), respectively. Moreover, comparison of the results with those determined using the damage index method (MSE) and another four damage identification methods (namely, mode shapes curvature, modal flexibility, uniform load surface curvature and stiffness method) indicates that the SSE is more sensitive to structural damage than the MSE method and in effect much more sensitive than the mode shapes curvature method, modal flexibility method, uniform load surface curvature method and stiffness methods. Details of the results obtained from five damage identification methods applied to the same sets of data by previous researchers can be found elsewhere [25,27]. For instance, the level of strength of the damage localization indices determined is different for the SSE and MSE methods. In the case of damage scenarios E-4, the maximum values of the normalized DI obtained from MSE were about 5.5 standard deviations for SET1 and 4.5 standard deviations for SET2 [25,27]. On the other hand, the maximum values of the normalized damage index determined from SSE were about 8.0 standard deviations for SET1 and 5.5 standard deviations for SET2 (see Figs. 20(b) and 21(b)). Similarly, in the case of damage scenario E-3, the SSE method was found to outperform the MSE for SET2 measurement data (see Figs. 20(a) and 21(a)). Finally, from the point of view of accuracy, the SSE method was found to be more precise than the MSE method. This can be observed from the normalized DI plots at 2 standard deviation levels for damage scenarios E-3 and E-4 in which the widths of the normalized DI were found to be wider for the MSE than the SSE method.

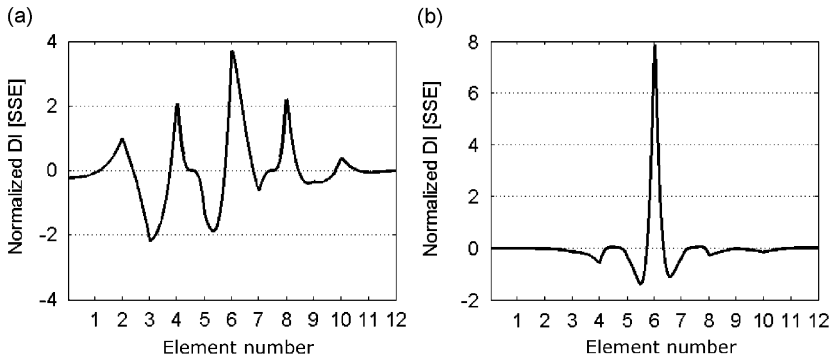

Fig. 20. Damage identification results from normalized response SSEs of the I-40 Bridge using SET1 modal data: (a) damage scenario E-3 and (b) damage scenario E-4.

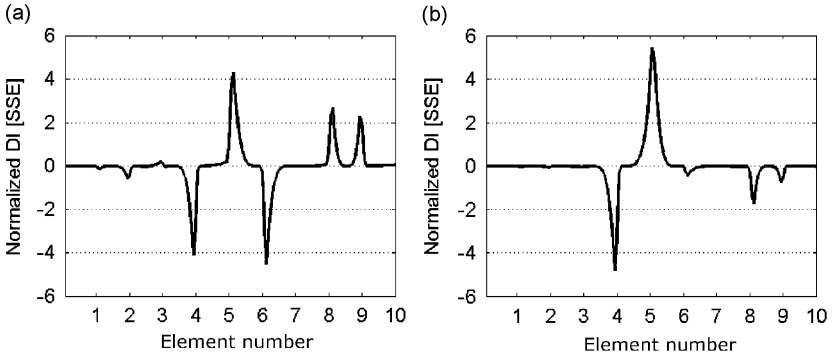

Fig. 21. Damage identification results from normalized response SSEs of I-40 Bridge using SET2 modal data: (a) from damage scenario E-3 and (b) from damage scenario E-4.

6. Conclusion

In this paper, a new vibration-based structural damage identification technique is proposed for identification and localization of structural damage in plate-like structures based on a non-model-based damage identification approach. The original contribution being made is that the SSE of the vibration response signal is systematically developed based on the MSV of moment and curvature response spectral density.

The effectiveness of the proposed method is demonstrated by conducting a detailed damage identification study on plate and beam elements using simulated damage conditions. The level of sensitivity and performance of the proposed method to changes in structural properties initiated by damage is illustrated by comparing the results from the proposed method with those obtained from existing methods, namely natural frequencies and MSE. The results from deterministic as well as statistically based damage indices clearly indicate remarkable performance of the proposed method as compared to the existing methods. This is because the proposed method utilizes broadband frequency information unlike its alternative counterparts which are limited to resonance frequency information. For instance, the relative sensitivity of the SSE to damage in plate elements is found to be about three times that of MSE and about twenty times that of modal flexibility and uniform surface although the results from the latter two parameters are not presented in this paper. Moreover, the proposed method can be applied to input–output as well as output-only damage identification problems. For the case of output-only problems, the only assumption made is that the excitation force is a stationary ergodic random process.

The experimental verification studies conducted in this paper validate the results obtained from the extensive numerical studies, namely that the SSE damage identification method is damage-sensitive, robust and reliable for structural damage identification and condition monitoring. Finally, the effects of high modal densities such as shear modes on the practical performance of the SSE-based damage identification have not been investigated in this paper. Similarly, further research is required to determine the effectiveness and limitations of the proposed SSE method to detecting and localizing structural damage near the boundaries and supports.

References

[1] S.W. Doebling, C.L. Farrar, M.B. Prime, D.W. Shevitz, Damage identification and health monitoring of structural and mechanical systems from changes in their vibration characteristics: a literature review, Los Alamos National Laboratory Report, LA-13070-MS, 1996.

[2] P. Cawley, R.D. Adams, The location of defects in structures from measurements of natural frequencies, *Journal of Strain Analysis for Engineering Design* 14 (1979) 49–57.

[3] A.K. Pandey, M. Biswas, M.M. Samman, Damage detection from changes in curvature mode shapes, *Journal of Sound and Vibration* 145 (1991) 321–332.
[4] A.K. Pandey, M. Biswas, Damage detection in structures using changes in flexibility, *Journal of Sound and Vibration* 169 (1994) 3–17.
[5] Q. Lu, G. Ren, Y. Zhao, Multiple damage location with flexibility curvature and relative frequency change for beam structures, *Journal of Sound and Vibration* 253 (2002) 1101–1114.
[6] Z. Zhang, A.E. Aktan, Application of modal flexibility and its derivatives in structural identification, *Research in Nondestructive Evaluation* 10 (1998) 43–61.
[7] D.V. Jauregui, C.R. Farrar, Comparison of damage identification algorithms on experimental modal data from a bridge, *Proceedings of the 14th International Modal Analysis Conference*, Vol. 2, Dearborn, Michigan, 1996, pp. 1423–1429.
[8] P. Cornwell, S.W. Doebling, C.R. Farrar, Application of the strain energy damage detection method to plate-like structures, *Journal of Sound and Vibration* 224 (1999) 359–374.
[9] H.Y. Hwang, C. Kim, Damage detection in structures using a few frequency response measurements, *Journal of Sound and Vibration* 270 (2004) 1–14.
[10] R.P.C. Sampaio, N.M.M. Maia, J.M.M. Silva, Damage detection using the frequency response function curvature method, *Journal of Sound and Vibration* 226 (1999) 1029–1042.
[11] T. Marwala, Fault identification using pseudomodal energies and modal properties, *Journal of Aircraft* 39 (2001) 1608–1617.
[12] S. Liberatore, G.P. Carman, Power spectral density analysis for damage identification and location, *Journal of Sound and Vibration* 274 (2004) 761–776.
[13] H.P. Chen, N. Bicanic, Assessment of damage in continuum structures based on incomplete modal information, *Computers & Structures* 74 (2000) 559–570.
[14] U. Lee, J. Shin, A structural damage identification method for plate structures, *Engineering Structures* 24 (2002) 1177–1188.
[15] Y.Y. Li, L. Cheng, L.H. Yam, W.O. Wong, Identification of damage locations for plate-like structures using damage sensitive indices: strain modal approach, *Computers & Structures* 80 (2002) 1881–1894.
[16] L.H. Yam, Y.Y. Li, W.O. Wong, Sensitivity studies of parameters for damage detection of plate-like structures using static and dynamic approaches, *Engineering Structures* 24 (2002) 1465–1475.
[17] D. Wu, S.S. Law, Damage localization in plate structures from uniform load surface curvature, *Journal of Sound and Vibration* 276 (2004) 227–244.
[18] M.K. Yoon, D. Heider, J.W. Gillespie Jr., C.P. Ratcliffe, R.M. Crane, Local damage detection using the two-dimensional gapped smoothing method, *Journal of Sound and Vibration* 279 (2005) 119–139.
[19] A.S.J. Swamidas, Y. Chen, Monitoring crack growth through changes of modal parameters, *Journal of Sound and Vibration* 186 (1995) 325–343.
[20] C.S. Krishnamoorthy, *Finite Element Analysis: Theory and Programming*, Tata McGraw-Hill, New Delhi, 1999.
[21] D.E. Newland, *An Introduction to Random Vibrations and Spectral Analysis*, second ed., Longman, New York, 1984.
[22] R. Szilard, *Theory and Analysis of Plates: Classical and Numerical Methods*, Prentice-Hall, Englewood Cliffs, NJ, 1974.
[23] ANSYS 8.0 User's Manual, ANSYS Inc., 2004.
[24] ARTeMIS Extractor 3.5, Structural Vibration Solutions A/S, Aalborg, Denmak.
[25] C.R. Farrar, W.E. Baker, T.M. Bell, E.M. Cone, T.W. Darling, T.A. Duffey, A. Eklund, A. Migliori, Dynamic characterization and damage detection in the I-40 Bridge over the Rio Grande, Los Alamos National Laboratory Report, LA-12767-MS, 1994.
[26] N. Stubbs, J.-T. Kim, C.R. Farrar, Field verification of a non-destructive damage localization and severity estimation algorithm, *13th International Modal Analysis Conference*, Vol. 1, 1995, pp. 210–218.
[27] C.R. Farrar, D.V. Jauregui, Comparative study of damage identification algorithms applied to a bridge: I. Experimental, *Smart materials and Structures* 7 (1998) 704–719.
[28] C.R. Farrar, D.V. Jauregui, Damage detection algorithms applied to experimental and numerical modal data from the I-40 Bridge, Los Alamos National Laboratory Report, LA-13074-MS, 1996.
[29] The I-40 Bridge modal data, 〈http://www.lanl.gov/projects/damage_id/data.shtml〉.